Interactions (2026) 247:158
https://doi.org/10.1007/s10751-026-02522-w

CONFERENCE PROCEEDING

Lead iron tungstate with partially ordered B-sites exhibiting relaxor ferroelectric and ferrimagnetic properties

Thien Thanh Dang[1] · Juliana Heiniger -Schell[1,2] · Eva Kröll[1] · Ian Chang Jie Yap[1] · Björn Dörschel[1] · Si Qi Jin[3] · Adeleh Mokhles Gerami[4] · Koen van Stiphout[5] · Doru Constantin Lupascu[1]

Received: 11 September 2025 / Accepted: 16 April 2026

Abstract
This work investigates atomic-scale partial B-site ordering in the complex perovskite relaxor lead iron tungstate, $Pb[Fe_{1-x}W_x]_{0.5}[Fe_{1/3+x}W_{2/3-x}]_{0.5}O_3$ ($0<x<1/3$), abbreviated as PFWO, using Time Differential Perturbed Angular Correlation (TDPAC) spectroscopy. The radioactive isotope ^{111m}Cd (decaying to ^{111}Cd) is employed as a sensitive tracer probe to explore the local electric and magnetic environments at atomic sites within the lattice. Temperature-dependent TDPAC measurements performed over a broad range (9–420 K) reveal the persistence of local electric field gradients at the Pb^{2+} sublattice in the face-centered cubic (*Fm-3 m*) structure. This observation indicates local symmetry breaking due to partial B-site ordering, wherein Fe^{3+} and W^{6+} ions exhibit a degree of site preference, and confirms the presence of short-range polar ordering characteristic of relaxor ferroelectric behavior. Moreover, the detection of a non-zero local magnetic field at the Pb site—where complete spin compensation would be expected in an ideal antiferromagnetic configuration—provides compelling evidence for ferrimagnetic ordering. This ferrimagnetism is attributed to partial B-site cation ordering, resulting in unequal sublattice magnetizations and incomplete spin cancellation. These findings highlight the critical role of atomic-scale B-site ordering in mediating the coexistence of relaxor ferroelectricity and ferrimagnetism in PFWO.

Keywords Combined hyperfine interaction · TDPAC · Relaxor ferroelectricity · Lead iron tungstate

✉ Thien Thanh Dang
thien.dang@uni-due.de

[1] Institute for Materials Science and Center for Nanointegration Duisburg-Essen (CENIDE), University of Duisburg-Essen, 45141 Essen, Germany

[2] European Organization for Nuclear Research (CERN), Geneva CH-1211, Switzerland

[3] Institut für Anorganische Chemie, Georg-August-Universität Göttingen, Tammannstraße 4, 37077 Göttingen, Germany

[4] School of Particles and Accelerators, Institute for Research in Fundamental Sciences (IPM), P.O. Box 19395-5531, Tehran, Iran

[5] Georg-August-Universität Göttingen, Friedrich-Hund-Platz 1, 37077 Göttingen, Germany

Published online: 23 April 2026

1 Introduction

Over the past several decades multiferroic materials have attracted significant attention due to their remarkable physical properties and promising potential for a wide range of technological applications [1]. These materials simultaneously exhibit two or more primary ferroic properties within the same phase including ferromagnetism ferroelectricity and ferroelasticity. Among multiferroics $A(B'B'')O_3$-type relaxor ferroelectrics are of interest because of their exceptionally high dielectric constants which are maintained over a broad temperature range [2, 3]. Within this class of materials, lead iron tungstate, $Pb[Fe_{1-x}W_x]_{0.5}[Fe_{1/3+x}W_{2/3-x}]_{0.5}O_3 (0<x<1/3)$ abbreviated as PFWO has emerged as a focal point of research due to its intriguing magnetoelectric coupling and relaxor behavior [4–6].

Lead iron tungstate (PFWO) was previously thought to crystallize in the disordered primitive cubic space group *Pm-3 m*(No. 221) [7–9], corresponding to the stoichiometry $PbFe_{2/3}W_{1/3}O_3$. Within this structural model, Fe and W cations are assumed to be randomly distributed across the B-sites of the perovskite lattice. In other words, Fe^{3+} and W^{6+} ions are evenly mixed throughout both B-site sublattices without any site preference, resulting in the absence of long-range cation ordering. This configuration, described as "disordered," maximizes the symmetry of the perovskite structure, producing a primitive cubic phase in which all B-sites are crystallographically equivalent [10]. This complete disorder has significant implications for the physical properties of the material. The magnetic behavior arises from the Fe^{3+} ions ($3d^5$, spin = 5/2), which are inherently magnetic, whereas the W^{6+} ions ($5d^0$, spin = 0) are non-magnetic. In a fully disordered lattice, the Fe^{3+} ions are randomly surrounded by W^{6+} ions, which dilutes the magnetic Fe–O–Fe superexchange pathways. As a result, magnetic interactions become frustrated, weakening or disrupting long-range magnetic order and often giving rise to antiferromagnetic or paramagnetic behavior. Likewise, the high symmetry inherent to the primitive cubic structure macroscopically favors a paraelectric state, as the random distribution of cations precludes the formation of coherent long-range electric dipole order. Therefore, if PFWO were to adopt the *Pm-3 m* structure, its symmetric electric and magnetic properties would severely limit its utility for functional applications that rely on ferroic ordering.

However experimental evidence has revealed that PFWO exhibits anomalous behavior that contradicts the predictions of a fully disordered model. Notably it demonstrates relaxor ferroelectric behavior characterized by the presence of local electric dipoles without long-range ordering typical of conventional ferroelectrics [11, 12]. In addition, PFWO displays ferrimagnetic properties, with unequal and partially cancelling magnetic moments [13]. Such a coexistence of strong relaxor ferroelectricity and ferrimagnetism is inconsistent with a completely disordered B-site arrangement, leading to considerable interest in understanding the underlying mechanisms responsible for these intriguing and unconventional properties.

A comprehensive structural investigation of PFWO single crystals, employing a combination of synchrotron X-ray diffraction and high-resolution electron microscopy over the temperature range of 100–450 K, has recently provided compelling evidence for partial, non-random occupation of Fe and W ions at distinct crystallographic sites [14]. Specifically, this study demonstrated that Fe and W ions exhibit a statistical preference for particular B-sites within the perovskite lattice, namely site B′ (4a) and site B″ (4b). Although the segregation is not complete, this partial site preference indicates the presence of B-site cation

ordering, distinguishing PFWO from a fully disordered perovskite structure. Quantitatively, the refined occupancies reveal that site 4a is occupied by approximately 69% Fe and 31% W, while site 4b contains about 64% Fe and 36% W. This distribution clearly shows that Fe and W ions are not equally dispersed across both sites, but rather display a significant tendency to favor specific sites, consistent with partial ordering [14]. Furthermore, Ivanov et al. determined that lead iron tungstate adopts the partly ordered face-centered cubic (FCC) space group *Fm-3 m* as shown in Fig. 1, with the general stoichiometry $Pb[Fe_{1-x}W_x]_{0.5}[Fe_{1/3+x}W_{2/3-x}]_{0.5}O_3$, where $0<x<1/3$. Within this structural model, partial B-site cation ordering is described as follows: Site 4a is occupied according to $Fe_{1-x}W_x$ ($x\approx0.31$), and site 4b follows $Fe_{1/3+x}W_{2/3-x}$ ($x\approx0.307$). These occupancy ratios correspond to partial B-site ordering. This finding confirms that the PFWO crystals investigated exhibit moderate but statistically significant partial B-site cation ordering, a structural feature that likely plays a critical role in the unusual magnetoelectric properties of the material.

Unlike conventional ferroelectric materials such as $BaTiO_3$ [15] or $BiFeO_3$ [16] which exhibit well-defined long-range ferroelectric order lead iron tungstate (PFWO) is characterized by only short-range polar ordering. In PFWO ferroelectricity arises from the formation of nanoscale regions known as polar nanoregions (PNRs) where local electric dipoles align along the [100] direction [14]. These dipoles primarily originate from the stereochemically

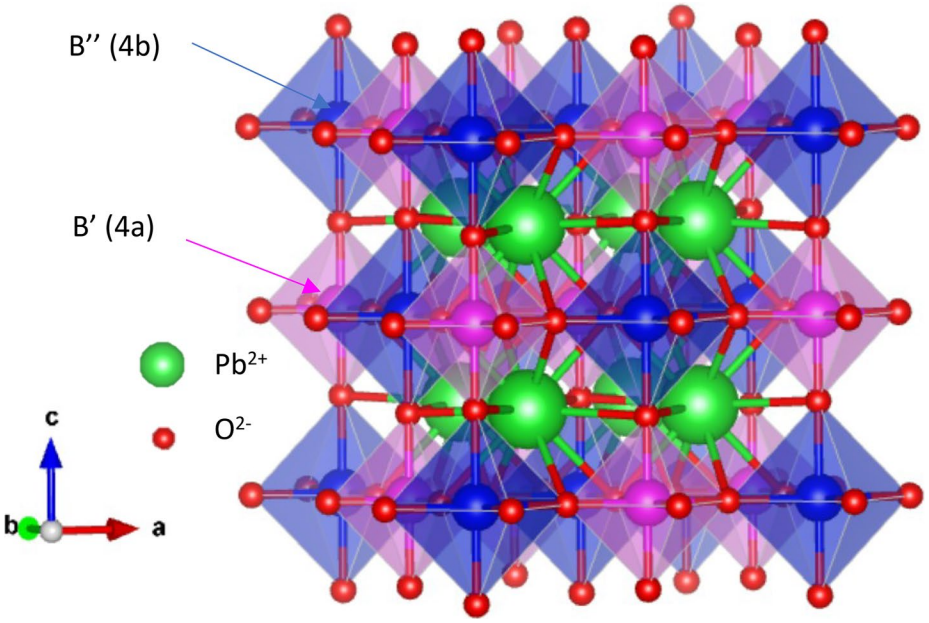

Fig. 1 The partly ordered face-centered cubic (FCC) space group *Fm-3 m* of $Pb[Fe_{1-x}W_x]_{0.5}[Fe_{1/3+x}W_{2/3-x}]_{0.5}O_3$ crystal. The figure is a structural representation, not a counted chemical diagram. It visually highlights two distinct B-sites labelled B′ and B″. The use of colored polyhedra is to illustrate that Fe and W occupy different kinds of sites, consistent with partial ordering: Site B′ (4a): 69% Fe, 31% W, Site B″ (4b): 64% Fe, 36% W. But the image does not attempt to show the exact number of Fe and W atoms — it is symbolic, not proportional. It is to be noticed that the figure does not label individual ions as Fe or W. It just marks two types of B-sites. We cannot count "2 blue = Fe and 1 pink = W" directly, because both B′ and B″ sites contain mixtures. So the Fe: W = 2:1 ratio is true for the whole crystal, but not fully in this small unit cell or visual block. This figure was re-constructed based the work of Ivanov et al. [14]

active $6s^2$ lone pair electrons of the Pb^{2+} ions which induce local structural distortions. However no coherent long-range alignment of these dipoles occurs throughout the crystal lattice [11, 12].

Although a variety of conventional characterization techniques have been employed to investigate PFWO, progress in fully understanding its ferroic behavior has been limited, largely due to its complex and partially frustrated magnetic structure [6]. Consequently, fundamental questions regarding the nature of its local relaxor ferroelectric ordering and the mechanisms of local electromagnetic coupling remain unresolved. To address these challenges, the application of advanced, site-specific characterization methods is adequate for probing the local structural and electronic environments at the atomic scale. In this regard, the Time Differential Perturbed Angular Correlation (TDPAC) technique [17, 18] offers a powerful approach by enabling the investigation of materials at the unit-cell level through the use of tracer probe ions. These probe ions such as ^{111m}Cd typically substitute into the lattice without significantly perturbing its intrinsic properties [19] allowing for highly sensitive detection of local electric field gradients and magnetic hyperfine interactions [20]. Such measurements provide valuable insights into the short-range ordering and dynamics of polar nanoregions in relaxor ferroelectrics like PFWO. Notably the TDPAC method has recently been employed to study magnetoelectric decoupling at the unit-cell level in bulk $BiFeO_3$ (BFO) using the ^{111m}Cd probe yielding critical information on local ferroic interactions [19]. In our study TDPAC measurements have been carried out over a wide temperature range encompassing all relevant structural and ferroic phase transitions [21, 22, 19]. Building on this approach, we propose to apply TDPAC with the ^{111m}Cd probe to PFWO to investigate its local relaxor ferroelectric properties and its complex magnetoelectric behavior.

2 Experimental details

The polycrystalline PFWO ceramic samples were synthesized using the two-stage solid-state columbite method, which is known to effectively suppress the formation of undesired secondary phases [23]. A detailed description of the synthesis procedure and structural characterization of PFWO is provided in the work of Kröll et al. [24]. In the present study, we employed the same preparation route (denoted as PFW2P85/90), involving a 2 wt% PbO excess, a calcination temperature of 850 °C, and a sintering temperature of 900 °C, in order to ensure consistency with the previously reported structural and functional properties of PFWO. The addition of a slight PbO excess is a standard approach to compensate for Pb volatilization during high-temperature processing and to promote phase purity, thereby minimizing the formation of secondary phases and preserving the desired perovskite structure. Following synthesis, the samples were ion-implanted with the radioactive probe isotope ^{111m}Cd at an implantation energy of 30 keV at the Ion Separator On-Line Device (ISOLDE) facility at CERN [25]. The projected implantation depth was estimated using the Stopping and Range of Ions in Matter (SRIM) simulation software [26], assuming a sample density of 9.03 g/cm³, as obtained from the HighScore Plus database [27], and an ion incidence angle of 0°. According to this simulation, the mean implantation depth of ^{111m}Cd in the PFWO is approximately 120 Å, as illustrated in Fig. 2. Subsequent to the implantation process, the TDPAC measurements were conducted at the ISOLDE Solid State Physics laboratory [28].

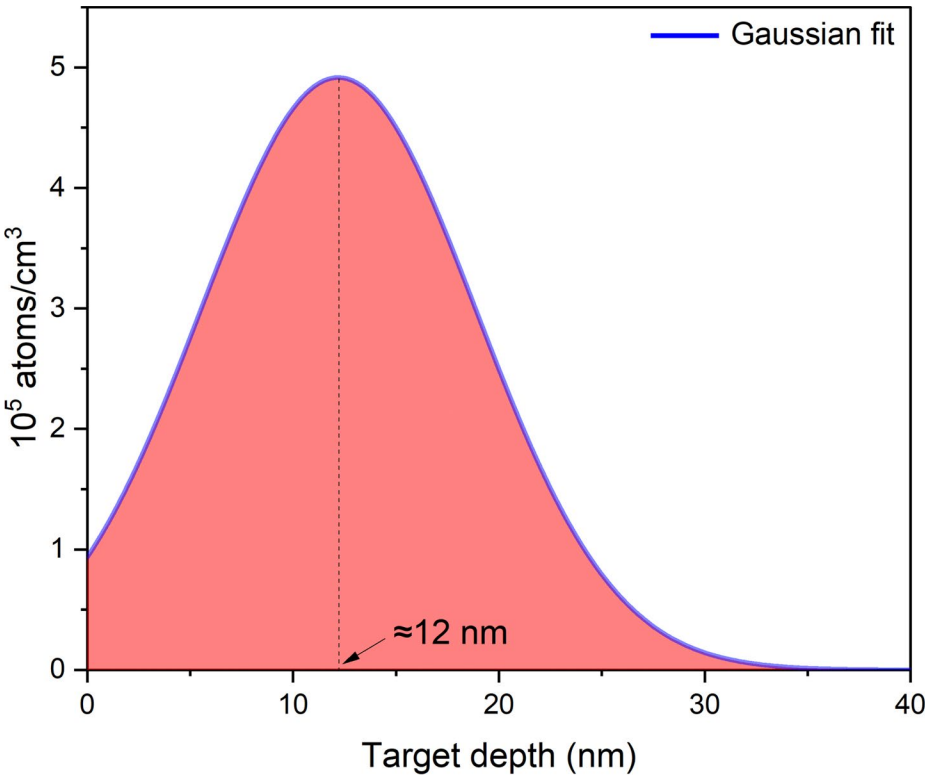

Fig. 2 Simulation of the distribution of the stopping range of implanted ^{111m}Cd ions into PFWO using SRIM 2008 [26]. The Gaussian fit (blue curve) shows a mean value at about 12 nm. This means that the pure beam of ^{111m}Cd, with an energy of 30 keV, after hitting the PFWO target at the incident angle about 0^o, will penetrate about 12 nm (d: penetrating depth) into the PFWO target

3 TDPAC formalism

Detailed descriptions of the Time Differential Perturbed Angular Correlation (TDPAC) technique and its theoretical formalism can be found in classic literature [29–32]. In the present study, we focus on outlining the TDPAC formalism as it applies to combined hyperfine interactions. In principle, the TDPAC technique exploits the angular correlation between two γ-rays emitted successively from the same radioactive nucleus. These γ-rays are detected by pairs of detectors positioned at specific angles, typically either perpendicular (90°) or collinear (180°) relative to each other. When all possible detector pair combinations in a typical six-detector configuration are considered, up to 30 single-coincidence spectra can be obtained [33]. For each coincidence spectrum, the background arising from accidental coincidences is systematically subtracted, thereby yielding the experimental count rate ratio R(t) (Eq.1). This function describes the time-dependent deviation between the coincidence count rates for the 180° and 90° detector orientations and serves as a direct representation of the hyperfine interactions within the sample.

$$R(t) = 2\frac{W\left(180^{\circ}, t\right) - W(90^{\circ}, t)}{W\left(180^{\circ}, t\right) + 2W(90^{\circ}, t)} = A_{22}G_{22}(t) \quad (1)$$

In Eq. (1), W(180°,t) denotes the 6th root of the product of all 180° coincidence spectra, while W(90°,t) denotes the 24th root of the product of the 90° coincidence spectra, both calculated after appropriate background subtraction and zero-point adjustment. The factor A_{22} represents the theoretical anisotropy coefficient, which is + 0.18 for the 151 keV – 245 keV γ-ray cascade of ^{111m}Cd [32]. It should be noted that this value is valid under the assumption of point-like detectors. To account for the finite dimensions of the actual detectors used in the experiments, the effective anisotropy coefficient must be corrected accordingly. For this purpose, the mean values of the anisotropy coefficients were determined through Monte Carlo simulations performed using the Monte program [34, 35]. The perturbation factor, $G_{22}(t)$, contains the time-dependent modulation of the angular correlation due to hyperfine interactions and thus the critical information about the local electromagnetic fields experienced by the probe nucleus. The explicit form of $G_{22}(t)$ depends on the nature of the hyperfine interaction. Detailed derivations for the perturbation factor in the cases of pure electric quadrupole and pure magnetic dipole interactions are comprehensively presented in the work of Butz et al., [31] and Dang et al., [19]. For the scenario of combined hyperfine interactions, the perturbation factor $G_{22}(t)$ takes the following form [21]:

$$G_{22}(t) = \sum {}_{i=1}^{m} f_i \left\{ a_{0i} + \sum {}_{n=1}^{30} a_{ni} \cos(\omega_{ni} t) \times \exp\left[-0.5 \left((\delta_i \omega_{ni} t)^p + (\omega_{ni} \tau_R)^2 \right) \right] \right\} \times \exp(-\lambda_i t) \quad (2a)$$

A detailed explanation of Eq. (2a) can be found in our previous publication [21]. In the present study, the PAC spectra were fitted using a single fraction that includes combined electric and magnetic hyperfine interactions, as implemented in the PACFit software [36]. No dynamic relaxation effects were considered. Consequently, Eq. (2a) reduces to:

$$G_{22}(t) = a_{0i} + \sum {}_{n=1}^{30} a_{ni} cos(\omega_{ni} t) \times \exp\left[-0.5 \left((\delta_i \omega_{ni} t)^p + (\omega_{ni} \tau_R)^2 \right) \right] \quad (2b)$$

The high fitting precision and reliability of PACFit have been validated in our earlier work [21]. The excellent agreement between the experimental spectra and the fitted curves ensures a clear separation of the magnetic contribution from the electric quadrupole interaction. As a result, the precession frequency (Larmor frequency) of the nuclear angular momentum in the magnetic field can be calculated using the following expression [32]:

$$\omega_L = -\frac{\mu}{I} B_{hf} \quad (3)$$

where B_{hf} is the local magnetic hyperfine field, $I = \frac{5}{2}\hbar$ is the nuclear spin angular momentum of the intermediate state of a radioactive nucleus ($\hbar$ is the reduced Planck's constant), and μ is the magnetic dipole moment of spin *I*.

The quadrupole interaction frequency is given by following expression [32]:

$$\omega_Q = \frac{eQ}{4I(2I-1)\hbar} V_{zz} \quad (4)$$

where e is the electron charge, Q the quadrupole moment of the intermediate state of the probe nucleus, V_{zz} is the largest z-component of the EFG. It relates to the other principal components and the asymmetry parameter of the EFG η by this relation [37]:

$$\eta = \frac{V_{xx} - V_{yy}}{V_{zz}} \tag{5}$$

The frequencies in Eqs. (3) and (4) are derived from the perturbation factor (Eq. 2b) that was used to fit the TDPAC spectra [19].

4 Experimental results and discussions

4.1 ^{111m}Cd probe site location

Following the implantation of ^{111m}Cd, the samples were annealed in air at 800 °C for 20 min prior to the TDPAC measurements. This post-implantation annealing process might change the probe distribution as shown in Fig. 2. It is expected that the implanted Cd^{2+} ions (coordination number XII) predominantly substitute for Pb^{2+} ions at the A-site of the perovskite lattice, as both ions share the same charge state (+ 2) and have comparable ionic radii, with Cd^{2+} and Pb^{2+} having ionic radii of 1.31 Å and 1.49 Å for a coordination of XII, respectively [40]. When Cd^{2+} occupies the Pb^{2+} site, it can serve as a sensitive probe for detecting both electric and magnetic hyperfine interactions arising from local lattice asymmetries in its direct vicinity, despite the overall face-centered cubic (*Fm-3 m*) symmetry of PFWO.

4.2 Electric quadrupole interaction

- *Above T_C (170 K):*

In this temperature range, the electric field gradient (EFG) would theoretically be expected to vanish due to the cubic lattice symmetry of PFWO and its paraelectric state. However, as shown by the R(t) spectra in Fig. 3a and corresponding Fast Fourier Transform (FFT) in Fig. 3b, a damped R(t) signal persists. The extracted quadrupole frequency fluctuates between 11 and 17 Mrad/s (Fig. 4a), with a pronounced peak appearing near the Néel temperature ($T_N \approx 380$ K), where the quadrupole frequency reaches approximately 19 Mrad/s. The existence of the secondary EFG above $T_C \approx 170$ K which is close to the $T_N$was ascribed to the spin–lattice interaction or magnetoelastic coupling effect [41, 42]. Particularly, the slight increase in the electric quadrupole frequency (ω_Q) in the vicinity of T_N is a well-documented phenomenon in materials undergoing magnetic phase transitions and is indicative of strong spin–lattice coupling [42]. Specifically, near the Néel temperature, the transition from an ordered antiferromagnetic (AFM) state to a disordered paramagnetic (PM) state involves significant reorientation of magnetic moments, which can locally distort the crystal lattice. These distortions enhance the EFG at the probe site, resulting in an increase in ω_Q. It should be emphasized that this enhancement of this secondary EFG is confined to the immediate vicinity of T_N.

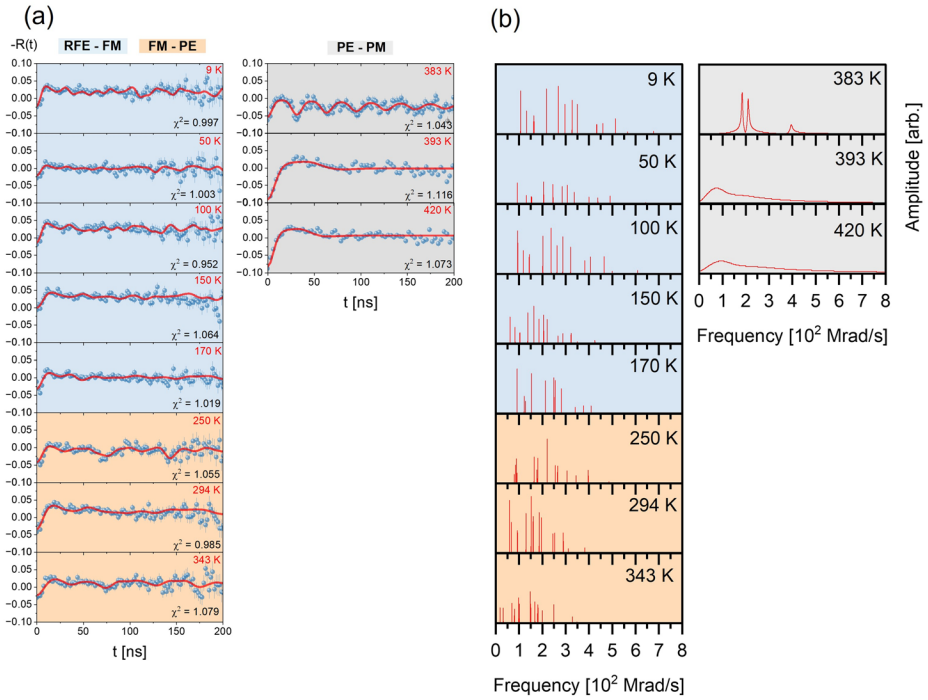

Fig. 3 (**a**) Temperature dependent R(t) spectra (RFE: relaxor ferroelectric, FM: ferrimagnetic, PE: paraelectric, PM: paramagnetic). The observed temperature-dependent shift of the R(t) baseline is a technical artifact of the ratio construction rather than an intrinsic physical effect. The hyperfine information is contained in the oscillatory part of the perturbation function, and the fitted interaction parameters remain unchanged within error when a constant offset term is included. Two different TDPAC spectrometers were used: PERM (9–383 K) [38] and KATAME (393 K, 420 K) [39]. Therefore, A_{22eff} obtained from two spectrometers are different. (**b**) FFTs of the R(t) fitted model curves

In PFWO, this pronounced spin–lattice interaction near the magnetic phase transition also influences the paraelectric–ferroelectric transition at T_C, as the two critical temperatures are relatively close [41]. In particular, the work of Kimura et al. demonstrated that in $TbMnO_3$ the ferroelectric phase emerges at or below the magnetic ordering temperature, indicating that the proximity of these two transitions is crucial for strong spin–lattice coupling near the magnetic phase transition. This system represents a well-known example of magnetically driven ferroelectricity, where the ferroelectric transition temperature is directly determined by the magnetic ordering temperature. Although PFWO is not a magnetically driven ferroelectric in the same sense, the relatively close proximity of the magnetic (T_N) and ferroelectric (T_C) transitions suggests that magnetic ordering can influence the local lattice distortions through spin–lattice or magnetoelastic coupling. Consequently, the onset of magnetic order may introduce an additional electric contribution to the local electric field gradient, which can affect the evolution of the paraelectric–ferroelectric transition near T_C. Consequently, the relaxor ferroelectric phase transition does not occur sharply at T_C, unlike in conventional ferroelectrics such as $BaTiO_3$, where the electric quadrupole frequency is expected to vanish completely at the Curie temperature [15].

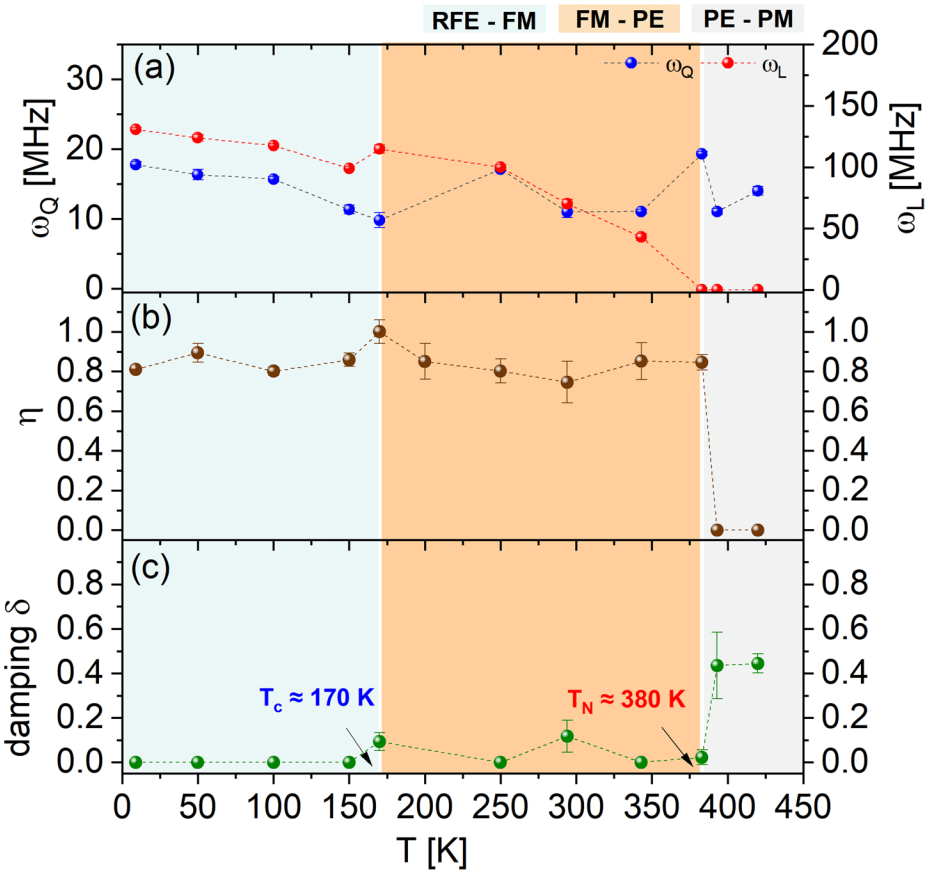

Fig. 4 (**a**) Temperature dependence of the quadrupole (ω_Q) and Larmor (ω_L) frequencies, (b) temperature dependence of the asymmetry parameter (η), (**c**) Temperature dependence of the damping parameter (δ). Some error bars are smaller than the plotted data points and are therefore not visible.

Furthermore, this strong spin–lattice coupling might affect the displacement of Pb^{2+} ions, which is the primary source of the EFG detected at the probe site. The coupling results in non-uniform distortions that lead to a broad distribution of transition frequencies, reflected by the high values of the damping factor δ, which reaches up to 45% near T_N (Fig. 4c). The large damping parameter observed in the paramagnetic phase reflects a broad distribution of EFGs arising from B-site chemical disorder, paramagnetic spin fluctuations, and relaxor-type local lattice distortions. Upon entering the magnetically ordered phase, the Fe^{3+} spins adopt a well-defined antiferromagnetic arrangement instead of fluctuating randomly as in the paramagnetic state. Because the magnetic exchange interactions depend sensitively on the Fe–O–Fe bond geometry, the establishment of long-range spin correlations stabilizes the surrounding oxygen framework through magnetoelastic (spin–lattice) coupling. As a result, the local lattice distortions become more uniform and fluctuate less within the PAC time window. Consequently, the ^{111m}Cd probe senses a more stable and well-defined local environment. The reduction of lattice fluctuations in the magnetically ordered state decreases the variety of local atomic configurations around the probe, resulting in a narrower distribution

of electric field gradients. As a result, the EFG distribution narrows significantly and the fitted damping parameter δ approaches zero. Here, "local atomic configurations" refer to the different possible arrangements of neighboring Fe^{3+} and W^{6+} cations and the associated local lattice distortions surrounding the Cd probe at the A-site. Each configuration produces a slightly different electric field gradient at the probe nucleus.

More importantly, the observation of non-zero electric quadrupole frequencies in the paraelectric phase—particularly near T_N—provides compelling evidence for the presence of partial B-site ordering between Fe and W cations. The static arrangement of Fe^{3+} and W^{6+} ions at the B-sites within this temperature range [14] disrupts the ideal symmetry of the *Fm-3 m* cubic structure by differentiating between distinct crystallographic sites. This local ordering enables the emergence of an observable relaxor ferroelectric phase transition, despite the overall cubic symmetry. However, this structural reorganization does not constitute a classical phase transition with a well-defined, abrupt boundary. Instead, it is better described as a gradual, diffusion-driven rearrangement of cations that occurs during slow cooling or under specific synthesis conditions [14]. In such a scenario, there is no singular temperature at which the lattice transitions sharply from a disordered to an ordered state. Rather, as the system cools, Fe^{3+} and W^{6+} ions progressively migrate toward energetically favorable sites (e.g., 4a and 4b positions) through atomic diffusion processes. This behavior is characteristic of relaxor ferroelectrics, such as PFWO. Relaxors are distinguished by their lack of long-range ferroelectric order and instead exhibit only short-range ordering in the form of nanoscale polar regions, known as polar nanoregions (PNRs), where local dipoles align. These regions do not extend coherently throughout the entire lattice as in conventional ferroelectrics. Consequently, relaxor ferroelectrics display broad, diffuse phase transitions and a pronounced frequency dependence in their dielectric response. Such properties arise from inherent structural or chemical disorder—such as mixed B-site cation occupancy—that disrupts the establishment of long-range polar coherence [43].

- *Below T_C (< 170 K)*: *relaxor ferroelectric order*.

In the temperature range below T_C, the electric quadrupole frequency ω_Q decreases gradually with increasing temperature up to approximately $T_C \approx 170$ K. After carefully fitting all R(t) spectra, the Curie temperature is now determined from a distinct decrease in ω_Q occurring near this temperature. The phase transition cannot be directly identified from the raw R(t) spectra because the electric quadrupole signal overlaps with the magnetic hyperfine interaction, making the change difficult to distinguish visually. However, by performing a careful fit of the spectra using the combined hyperfine interaction model, the electric quadrupole component (ω_Q) can be reliably separated from the magnetic contribution. The temperature evolution of ω_Q extracted from these fits clearly indicates the presence of the phase transition. This phase transition temperature (170 K) is consistent with previously reported transition temperatures in PFWO obtained by structural and magnetic measurements [10, 6], as well as with temperature-dependent dielectric studies, which place the relaxor transition in a similar temperature range [24]. Based on the observed behavior of ω_Q, the transition can be classified as a first-order transition close to a second-order character, consistent with the behavior discussed in our previous study [19].

In this temperature range, the EFG decreases gradually with increasing temperature due to the thermal disorder. Specifically, when the temperatures increase, thermal fluctuations

increasingly randomize the off-center displacements of the Pb^{2+} ions that originate from the stereochemically active $6s^2$ lone pair. Although the magnitude of the local Pb displacement may remain finite, its orientation becomes progressively more disordered due to thermal motion. As a result, the effective local polarization sensed by the ^{111m}Cd probe decreases, leading to a gradual reduction of the electric field gradient and thus of the quadrupole frequency ω_Q with increasing temperature.

The relatively broad evolution of ω_Q near T_C is consistent with the intrinsic nature of relaxor ferroelectrics, which are characterized by short-range polar ordering, diffuse phase transitions, and local structural disorder that inhibit the formation of long-range ferroelectric coherence [43]. In PFWO, the situation is further complicated by the coexistence of relaxor ferroelectricity and antiferromagnetic order within this temperature range. Under these conditions, the R(t) spectra represent the superposition of electric and magnetic hyperfine interactions and therefore exhibit the characteristic features of combined-interaction spectra, consistent with simulations reported in our previous study [21].

Although the relaxor transition is not sharply resolved in the R(t) spectra themselves the TDPAC results are consistent with structural studies reported byIvanov et al. using synchrotron X-ray diffraction and high-resolution electron microscopy over the temperature range 100 –450 K [14]. That work demonstrated that Pb^{2+} ions undergo off-center displacements along the [100] direction due to the stereochemically active $6s^2$ lone pair electrons, resulting in local electric polarization along [100], rather than along [111] as previously assumed [10]. Importantly, the Pb displacement persists across the investigated temperature range and evolves gradually with temperature, without a sharp structural anomaly at the transition temperature. The temperature dependence of the Pb displacement reported by Ivanov et al. correlates well with the evolution of the electric quadrupole frequency ω_Q observed in the present work. This agreement further supports the conclusion that the ^{111m}Cd probe substitutes predominantly at the Pb^{2+} site and is therefore sensitive to the local structural distortions associated with the relaxor ferroelectric behavior of PFWO.

We explicitly acknowledge the possibility of alternative sources contributing to the observed electric field gradient (EFG), such as B-site chemical disorder or local relaxation of the implanted probe. However, because the ^{111m}Cd probe substitutes at the Pb - site, it is comparatively less sensitive to the partially disordered Fe/W distribution on the B-site than a probe located directly on the B-site. In addition, the fitting of the R(t) spectra using a single fraction (i.e., assuming one dominant EFG environment) yields consistently good agreement with the experimental data, as reflected by the obtained χ^2 values. These results indicate that the PAC spectra can be adequately described by a single effective EFG component. Therefore, although local B-site disorder cannot be completely excluded as a contributing factor, the observed temperature dependence of the EFG is most consistently interpreted in terms of relaxor-related local structural distortions.

The partial ordering of Fe and W cations at the B-site is fundamental to understanding the relaxor ferroelectric behavior of PFWO—a phenomenon that has previously been challenging to interpret. The ferroelectric order in PFWO arises primarily from subtle off-center displacements of the lead (Pb^{2+}) ions, driven by their stereochemically active lone pair electrons. Although both Pb^{2+} and the implanted Cd^{2+} probe occupy the A-site, their displacement behavior is intrinsically linked to the structural and electronic environment of the B-site due to local electric field variations, octahedral distortions, and temperature-dependent effects. First, local electric field variations arise when Fe^{3+} and W^{6+} ions are par-

tially ordered, resulting in an anisotropic and non-uniform electrostatic environment. This asymmetry influences the extent of Pb^{2+} cation displacements, as the Pb lone pair electrons interact with the surrounding oxygen anions that are themselves coordinated to the Fe/W cations. Second, octahedral distortions occur as a consequence of B-site ordering, which alters the tilt, rotation, and size of the FeO_6 and WO_6 octahedra. These structural changes modify the positions of the coordinating oxygen atoms and, consequently, the Pb–O bonding network, thereby affecting the magnitude and direction of Pb off-centering. Third, temperature plays a significant role: as temperature increases, cation disorder on the B-site may become more pronounced and lattice vibrations tend to reduce the net Pb displacement amplitude. The gradual weakening of local B-site ordering at elevated temperatures diminishes the symmetry-breaking field that stabilizes the off-center position of Pb^{2+} ions. The indirect effect of B-site partial ordering on the Pb displacement along the [100] crystallographic direction has been demonstrated in Fig. 5 of Ivanov et al. [14], where the thermal evolution of the Pb shift correlates with the degree of Fe/W ordering. Taken together, these factors show that the partially ordered (Fe/W) B-site plays a pivotal role in stabilizing the relaxor ferroelectric state of PFWO. This relationship has been effectively probed in the present study by the ^{111m}Cd nuclei, which are believed to substitute at the Pb^{2+} site and thus sensitively reflect the local structural distortions and electric field variations that underpin the relaxor behavior.

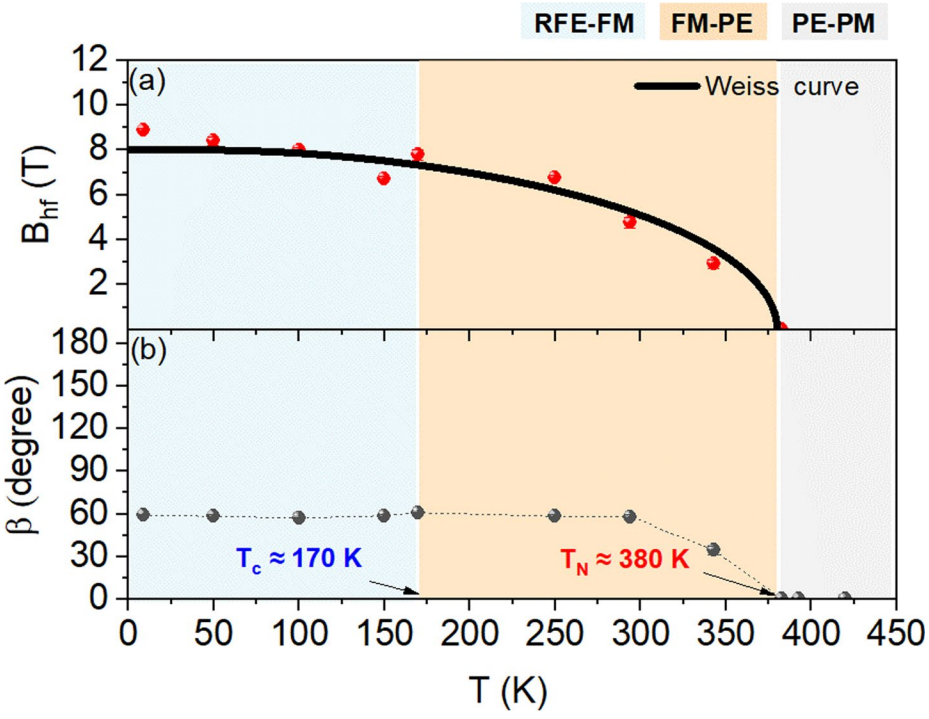

Fig. 5 (**a**) Temperature dependent hyperfine magnetic field. The fitting curve is derived from the analytical solution of the Weiss equation [21], (**b**) Temperature independent Euler angle β (angle between the main component EFG V_{zz} and locally effective B_{hf}). The error bars are smaller than the plotted data points and are therefore not visible

4.3 Local magnetic field at the non-magnetic Pb sublattice site (from 9 K to 378 K) – ferrimagnetic order

In this temperature range, two distinct ferroic phase transitions can be identified as the system cools through the Néel temperature ($T_N \approx 380$ K, corresponding to the paramagnetic–antiferromagnetic transition) and the Curie temperature ($T_C \approx 170$ K, corresponding to the paraelectric–ferroelectric transition). Below T_N, the TDPAC spectra clearly exhibit features characteristic of combined hyperfine interactions (CHI). Figure 3a & b present the R(t) spectra for CHI measured at the Cd probe site, along with their corresponding Fast Fourier Transforms (FFTs) for various temperatures up to 380 K.

The steeply declining R(t) spectra observed for CHI arise from the superposition of well-defined electric and magnetic hyperfine interactions [21]. It is important to note that this amplitude decline is not due to a broad distribution of interaction frequencies; indeed, the magnetic interaction frequency (Larmor frequency) and the electric quadrupole frequency are both well resolved, with the damping factor approaching zero below T_N (see Fig. 4c). Although the R(t) spectra below T_N appear superficially similar to those above T_N, they differ fundamentally in origin. Above T_N, the spectra reflect pure electric quadrupole interactions with a broad distribution of quadrupole frequencies due to local structural disorder, whereas below T_N the spectra reflect coherent combined electric and magnetic interactions. As a result the first phase transition (paramagnetic–antiferromagnetic) is not sharply visible in the R(t) spectra themselves—unlike the clear signatures often seen in materials such as $BiFeO_3$ [22, 21]—but is instead better visible in the changes in the shape and frequency amplitudes of the corresponding FFTs. For CHI, the FFTs should theoretically display multiple peaks corresponding to the 15 transition frequencies permitted for spin $I = 5/2$. In practice, however, only transition frequencies with the largest amplitudes are clearly resolved, while low-amplitude frequencies are not distinguishable in the spectra.

The evolution of the magnetic hyperfine field as a function of temperature provides further confirmation of the antiferromagnetic transition. As shown in Fig. 5, the magnitude of the local magnetic field decreases continuously with increasing temperature and vanishes near $T_N \approx 380$ K, in excellent agreement with the analytical solution of the Weiss-Brillouin function [21].

One notable characteristic of the CHI regime is the pronounced asymmetry of the electric field gradient (EFG), as indicated by the asymmetry parameter (η) in Fig. 4b. This asymmetry arises from the influence of local magnetic field on the charge distribution surrounding the probe nucleus leading to an EFG that deviates significantly from axial symmetry [22, 21].

The orientation of the effective local magnetization with respect to the electric polarization direction [100] has been determined to be $\beta \sim 58°$ (Fig. 5b), which is close to the crystallographic angle of 54.73°, corresponding to the angle between the [100] and [111] directions, as illustrated schematically in Fig. 6. This observation suggests that the effective magnetization vector is likely oriented along the crystallographic direction [111]. However, local B-site disorder may induce a rotation of V_{ZZ}, thereby limiting the precision of the directional analysis. Consequently, the β angle alone does not uniquely determine the magnetization direction. Density functional theory (DFT) calculations will be carried out in future work to determine the magnetization direction more accurately.

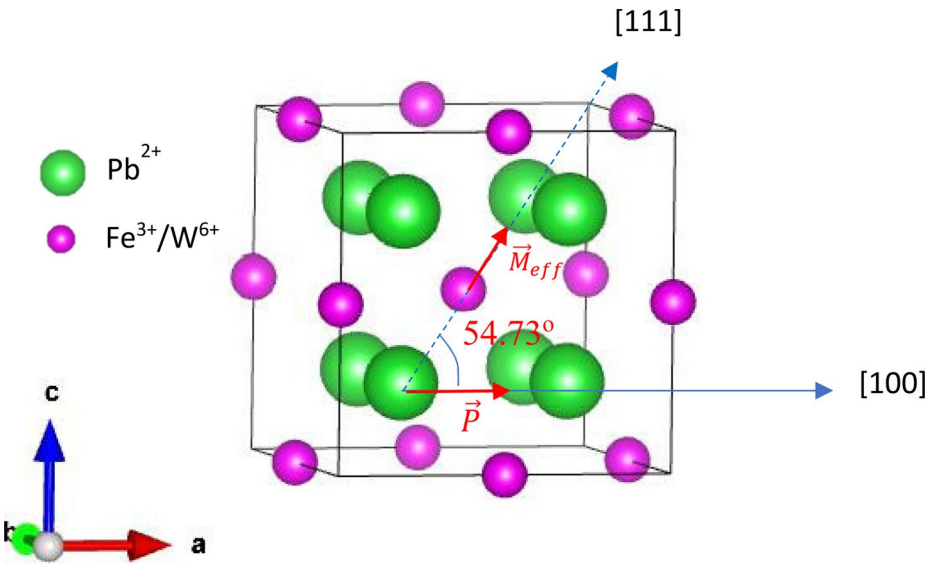

Fig. 6 The illustrated direction between effective magnetization [111] and electric polarization [100]. The experimental value is ~58°

When ^{111m}Cd occupies the A-site in a perovskite structure—for example, the Bi site in $BiFeO_3$—it typically detects no net local magnetic field due to the complete compensation of magnetic moments resulting from antiferromagnetic (AFM) ordering [19]. In contrast, the observation of a non-zero local magnetic field at the Pb site in PFWO indicates that the system exhibits ferrimagnetic ordering below T_N. This ferrimagnetism arises from the partial ordering of Fe and W cations on the B-site. Specifically, if the Fe^{3+} ions (which are magnetic) and W^{6+} ions (which are non-magnetic) are not completely randomly distributed but instead exhibit a degree of site preference—such that Fe^{3+} preferentially occupies one B-site (e.g., 4a) and $W^{6+}$the other (e.g., 4b)—the resulting arrangement breaks the perfect spin compensation typical of an ideal AFM structure. In this configuration, the two sublattices possess unequal net magnetic moments, leading to partial cancellation of opposing spins and a residual net magnetization characteristic of ferrimagnetic order [14, 44]. This ferrimagnetic behavior has also been independently confirmed through vibrating sample magnetometry (VSM) measurements, as reported in our previous study [24], further supporting the conclusion that the partial B-site ordering in PFWO drives the emergence of ferrimagnetism below T_N.

Our results are consistent with previous ^{57}Fe Mössbauer spectroscopy studies [4], which reported magnetically nonequivalent Fe environments arising from partial Fe/W ordering, in some cases leading to the observation of two magnetic sextets (from two unbalanced Fe subsystems due to partial Fe/W ordering). While Mössbauer spectroscopy resolves Fe-site-specific hyperfine fields, the present TDPAC measurements probe the transferred magnetic field at the A-site, providing complementary evidence for incomplete magnetic compensation in PFWO. As such, TDPAC naturally averages contributions from both Fe subsystems (averages over surrounding Fe/W configurations) and does not necessarily resolve multiple magnetic components at the A-site (their fields differ in magnitude but not enough to form

two resolved A-site hyperfine components), even when Mössbauer spectroscopy does so at the Fe site. The observation of a single combined hyperfine interaction at the Pb site in our study is therefore fully consistent with the Mössbauer evidence for unequal Fe sublattice magnetizations and ferrimagnetic ordering induced by partial B-site cation order.

5 Conclusions

In this study, we investigated the local electromagnetic environment in lead iron tungstate (PFWO) using ^{111m}Cd time-differential perturbed angular correlation (TDPAC) spectroscopy. The results indicate that the relaxor-like ferroelectric behavior of PFWO is closely related to the partial ordering of Fe and W cations at the B-site. This local structural arrangement influences the electric field gradient sensed by the ^{111m}Cd probe substituting at the Pb^{2+} site, providing local-scale information that is consistent with the presence of relaxor-type polar distortions in the material.

In addition, the observation of a finite local magnetic hyperfine field at the Pb site below the Néel temperature (T_N) suggests incomplete magnetic moment compensation at the A-site, which is compatible with ferrimagnetic ordering in PFWO. The observed ferrimagnetic behavior can be attributed to the partial, non-random distribution of Fe^{3+} and W^{6+} ions over the two B-site sublattices of the perovskite structure. This partial B-site ordering leads to unequal magnetic sublattices and therefore to incomplete spin compensation.

Taken together, the TDPAC results provide supporting local evidence consistent with the coexistence of relaxor-like electric behavior and ferrimagnetic ordering in PFWO. These findings highlight the important role of partial B-site ordering in influencing the interplay between structural and magnetic properties in this system and offer insight into how local cation ordering may contribute to the multifunctional behavior of complex perovskite oxides.

Supplementary Information The online version contains supplementary material available at https://doi.org/10.1007/s10751-026-02522-w.

Acknowledgements Financial support was provided by the Federal Ministry of Research, Technology and Space (BMFTR) through Grants No. 05K22PGA and 05K22PGB, alongside support from the ISOLDE collaboration. D.C.L. acknowledges support by the Deutsche Forschungsgemeinschaft through project 406710712. We acknowledge the support of the European Union's Horizon Europe Framework research and innovation programme under grant agreement no. 101057511 (EURO-LABS) and of the European Union's Horizon 2020 Framework research and innovation program under grant agreement no. 654002 (ENSAR2). Discussions with V.V. Shvartsman are highly acknowledged. We acknowledge the support of FCT- Portugal, projects UIDP/04349/2020 and 2024.00223.CERN, funded by RE-C06-i06.m02 – "Strengthening International Partnerships in Science, Technology and Innovation" of the PRR, through the agreement between EMRP and FCT as intermediate beneficiary (https://doi.org/10.54499/2024.00223.CERN).

Author contributions TTD performed the implantations, TDPAC experiments, data analysis and wrote the entire manuscript. JH-S contributed to the discussions and supervised the data analysis. EK prepared the samples. JH-S, I C J Y, BD, SQJ, AMG and KvS provided technical support during the implantations and TDPAC expriments. DCL supervised the work and contributed to the discussions.

Funding Open Access funding enabled and organized by Projekt DEAL.

Data availability No datasets were generated or analysed during the current study.

Declarations

Competing interests The authors declare no competing interests.

Data handling The data will be stored at CDS (CERN library repository).

References

1. Nicola, Spaldin, A., Fiebig, M.: The Renaissance of Magnetoelectric Multiferroics. Science. **309**, 391–392 (2005). https://doi.org/10.1126/science.1113357
2. Tinte, S., Burton, B.P., Cockayne, E., Waghmare, U.V.: Origin of the relaxor state in Pb(BxB1-x')O3 perovskites. Phys. Rev. Lett. **97**, 137601 (2016)
3. Raevskii, I.P., Sarychev, D.A., Bryugeman, S.A., Reznichenko, L.A., Shilkina, L.A., Razumovskaya, O.N., et al.: Study of cation ordering and magnetic phase transitions in ternary Fe-containing perovskite oxides by Mössbauer spectroscopy. Crystallogr. Rep. **47**, 1012–1015 (2002)
4. Koroleva, A.F., Bush, A.A., Kamentsev, K.E., Shkuratov, V.Y., Ivanov, S.A., Cherepanov, V.M., et al.: Synthesis, X-ray Diffraction Characterization, Mössbauer Spectroscopy, and Dielectric Properties of Solid Solutions in the PbFe2/3W1/3O3–PbSc2/3W1/3O3 System. Inorg Mater **54**, 288–294 (2018)
5. Kleemann, W., Shvartsman, V.V., Borisov, P., Kania, A.: Coexistence of antiferromagnetic and spin cluster glass order in the magnetoelectric relaxor multiferroic PbFe0.5Nb0.5O3. Phys. Rev. Lett. **105**, 257202 (2010)
6. Shivaraja, I., Matteppanavar, S., Rayaprol, S., Angadi, B.: Evidence of weak ferromagnetic and antiferromagnetic interaction at low temperature in Pb(Fe2/3W1/3)O3 multiferroic. Physica B: Condensed Matter **561**, 114–120 (2019)
7. Ye, Z.-G., Schmid, H.: Electric field induced effect on the optical, dielectric and ferroelectric properties of $Pb(Fe_{2/3}\ W_{1/3})O_3$ single crystals. Ferroelectrics **162**(1), 119–133 (1994)
8. Ye, Z.-G., Schmid, H.: Growth from high temperature solution and characterization of $Pb(Fe_{2/3}W_{1/3})O_3$ SINGLE crystals. J. Cryst. Growth **167**, 628–637 (1996)
9. Ye, Y., Toda, Z.-G., Sato, K., Kita, M., E., Schmid, H.: Synthesis, structure and properties of the magnetic relaxor ferroelectric Pb(Fe2/3W1/3)O3 [PFW]. J. Korean Phys. Soc. **32**, S1028–S1031 (1998)
10. Ivanov, S.A., Eriksson, S.-G., Tellgren, R., Rundlöf, H.: Neutron powder diffraction study of the magnetoelectric relaxor Pb(Fe2/3W1/3)O3. Materials Research Bulletin **39**(Issues 14–15), 2317–2328 (2004). https://doi.org/10.1016/j.materresbull.2004.07.025
11. Shvartsman, Y., Kania, D., Kleemann, W., Pirc, R.: Relaxor ferroelectrics. J. Appl. Phys. **101**, 084105 (2007). https://doi.org/10.1063/1.2717563
12. Tripathy, S.N., Das, A., Sanyal, P., Choudhary, R.N.P., Banerjee, A.: Relaxor ferroelectric and magnetic properties of PbFe1/2W1/2O3 multiferroic ceramics. J. Appl. Phys. **106**, 093517 (2009). https://doi.org/10.1063/1.3257683
13. Yusuf, S.M., Singh, K.J., Siruguri, V.: Magnetic properties of Pb(Fe1/2W1/2)O3: Evidence for ferrimagnetic ordering. Phys. Rev. B **66**, 064414 (2002). https://doi.org/10.1103/PhysRevB.66.064414
14. Ivanov, S.A., Stash, A.I., Riekehr, L., et al.: Structure of $Pb(Fe_{2/3}W_{1/3})O_3$ single crystals with partial cation order. Sci Rep **10**(1), 14567 (2020). https://doi.org/10.1038/s41598-020-71438-4
15. M.E., Lines, Glass, A.M.: Principles and Applications of Ferroelectrics and Related Materials. Clarendon, Oxford (1977)
16. Catalan, G., Scott, J.F.: Physics and applications of bismuth ferrite. Adv. Mater. **21**, 2463 (2009). https://doi.org/10.1002/adma.200802849
17. Forker, M.: Perturbed Angular Correlations as A Tool in Solid State Physics, In: Bethge, K., Baumann, H., Jex, H., Rauch, F. (eds) Nuclear Physics Methods in Materials Research, Vieweg+Teubner Verlag (1980). https://doi.org/10.1007/978-3-322-85996-9_11

18. Schell, J., Marschick, G.: TDPAC Studies of Local Defects and Phenomena in Ferroics and Multiferroics. Crystals **9**(12), 611 (2019). https://doi.org/10.3390/cryst9120611
19. Dang, T.T., et al.: Magnetoelectric Decoupling in Bismuth Ferrite. Phys. Rev. Lett. **134**, 216702 (2025). https://doi.org/10.1103/PhysRevLett.134.216702
20. Rasera, R.L., Catchen, G.L.: Perturbed angular correlation (PAC) spectroscopy as a tool for the study of ferroelectrics. Ferroelectrics **150**(1), 151 (1993). https://doi.org/10.1080/00150199308008701
21. Dang, T.T., Schell, J., Boa, A.G., Lewin, D., Marschick, G., Dubey, A., Escobar-Castillo, M., Noll, C., Beck, R., Zyabkin, D.V., Glukhov, K., Yap, I.C.J., Gerami, A.M., Lupascu, D.C.: Temperature dependence of the local electromagnetic field at the Fe site in multiferroic bismuth ferrite. Phys. Rev. B **106**, 054416 (2022). https://doi.org/10.1103/PhysRevB.106.054416
22. Schell, J., et al.: Strong magnetoelectric coupling at an atomic nonmagnetic electromagnetic probe in bismuth ferrite. Phys. Rev. B. **105**, 094102 (2022). https://doi.org/10.1103/PhysRevB.105.094102
23. Swartz, S.L., Shrout, T.R.: Fabrication of perovskite lead magnesium niobate. Mater. Res. Bull. **17**, 1245–1250 (1982)
24. Eva Kröll, Vladimir, V., Shvartsman; Doru, C., Lupascu: Juliana Schell; Soma Salamon; Heiko Wende, Effect of Excess Lead Oxide and Thermal Treatment on Dielectric and Magnetic Properties of Pb(Fe2/3W1/3)O3, 2021 IEEE International Symposium on Applications of Ferroelectrics (ISAF) | 978-1-6654-0444-0/20/$31.00 ©2021 IEEE | https://doi.org/10.1109/ISAF51943.2021.9477333
25. Catherall, R., et al.: The ISOLDE facility. J. Phys. G: Nucl. Part. Phys. **44**, 094002 (2017). https://doi.org/10.1088/1361-6471/aa7eba
26. Ziegler, JF.: SRIM-2008 software package, url: http://www.srim.org
27. HIGHSCORE PLUS: Version 4.7 (4.7.0. 24755). PANalytical B V (2017)
28. Johnston, K., et al.: The solid state physics programme at ISOLDE: recent developments and perspectives. J. Phys. G: Nucl. Part. Phys. **44**, 104001 (2017). https://doi.org/10.1088/1361-6471/aa81ac
29. Abragam, A., Pound, R.V.: Influence of electric and magnetic fields on angular correlations. Phys. Rev., 92, 943 (1953)
30. Frauenfelder, H., Steffen, R.M., Alpha-: Beta-, and Gamma-Ray Spectroscopy, edited by K. Siegbahn-North Holland, Amsterdam, Vol. 2. (1966)
31. Butz, T.: Analytic perturbation functions for static interactions in perturbed angular correlations of γ -rays. Hyperfine Interact. **52**, 189 (1989)
32. Schatz, G., Weidinger, A.: Nuclear Condensed Matter Physics—Nuclear Methods and Applications. John Wiley, Chichester (1996)
33. Danielsen, E., et al.: Structure of metal site in azurin, Met121 Mutants of Azurin, and Stellacyanin investigated by 111mCd perturbed angular correlation (PAC). J. Biol. Chem. **270**, 573 (1995). https://doi.org/10.1074/jbc.270.2.573
34. Nédélec, R.: Seltene Erden in GaN und ZnO untersucht mit der PAC-Methode, Dissertation in Physik, Universität Bonn, (2007)
35. Knichel, W.: Monte-Carlo-Simulation der Öffnungswinkelkorrektur der Detektoren der Zwölf-Detektor-Apparatur; VAX Quellcode Version, (1995)
36. Cavalcante, J., Forker, M.: PACFit with spin selection 2.0.0 (Build 342).
37. Lerf, A., Butz, T.: Nuclear quadrupole interactions in compounds studied by time differential perturbed angular correlations/distributions. Hyperfine Interact. **36**, 275–370 (1987). https://doi.org/10.1007/BF02395636
38. Jäger, M., Iwig, K., Butz, T.: A user-friendly fully digital TDPAC-spectrometer. Hyperfine Interact. **198**, 167–172 (2010). https://doi.org/10.1007/s10751-010-0201-8
39. Nagl, M., Nagl, U., Vetter, M., Uhrmacher, Hofsäss, H.: A new all-digital time differential γ-γ angular correlation spectrometer. Rev. Sci. Instrum. **81**, 073501 (2010)
40. Shannon, R.D.: Revised effective ionic radii and systematic studies of interatomic distances in halides and chalcogenides. Acta Cryst. A. **32**, 751 (1976). https://doi.org/10.1107/S0567739476001551
41. Kimura, T., Goto, T., Shintani, H., et al.: Magnetic control of ferroelectric polarization. *Nature* 426, 55–58 (2003). https://doi.org/10.1038/nature02018
42. Eerenstein, W., Mathur, N., Scott, J.: Multiferroic and magnetoelectric materials. Nature. **442**, 759–765 (2006). https://doi.org/10.1038/nature05023
43. Bokov, A.A., Ye, Z.G.: Recent progress in relaxor ferroelectrics with perovskite structure. J. Mater. Sci. **41**, 31–52 (2006). https://doi.org/10.1007/s10853-005-5915-7
44. Isupov, V.A.: Peculiarities of the $PbB^{2+}{}_{2/3}B^{6+}{}_{1/3}O_3$ perovskites. Ferroelectrics. **315**, 149–161 (2005)